Individual Tree Segmentation Based on Mean Shift and Crown Shape Model for Temperate Forest

Eduardo Tusa, *Graduate Student Member, IEEE*, Jean-Matthieu Monnet, Jean-Baptiste Barré, Mauro Dalla Mura, *Senior Member, IEEE*, Michele Dalponte, *Senior Member, IEEE*, and Jocelyn Chanussot, *Fellow, IEEE*

***Abstract*— Light detection and ranging (LiDAR) provides high-resolution geometric information for monitoring forests at individual tree crown (ITC) level. An important task for ITC delineation is segmentation, and previous studies showed that the adaptive 3-D mean shift (AMS3D) algorithm provides effective results. AMS3D for ITC segmentation has three components for the kernel profile: shape, weight, and size. In this letter, we present an AMS3D approach based on the adaptation of the kernel profile size through an ellipsoid crown shape model. The algorithm parameters are estimated based on allometry equations derived from 22 forest plots in two study sites. After computing the mean shift (MS) vector, we initialize the parameters of the ellipsoid crown shape model to derive the kernel profile size, and further tested two crown shape models for adapting the size of the superellipsoid (SE) kernel profile. These schemes are compared with two other MS algorithms with and without kernel profile size adaptation. We select the best algorithm output per plot based on the maximum F1-score. The ellipsoid crown shape model with a SE kernel profile of $n = 1.5$ presents the highest recall and the best Jaccard index, especially for conifers.**

***Index Terms*— Adaptive 3-D mean shift (AMS3D), conifers, crown shape model, individual tree crown (ITC) segmentation, light detection and ranging (LiDAR).**

I. Introduction

DECISION-SUPPORT systems for forest management rely on stand attribute information by collecting data on the ground in a field survey [1]. Field-based inventories are time-consuming and labor-intensive to be collected, providing rough estimates of stand attributes with typical sampling limitations because of terrain or vegetation factors [2]. Remote sensing based tools, in particular, individual tree level analysis, could contribute to producing more precise inventories; for instance, Crowther *et al.* [3] estimated the world's tree population in 3.04 trillion based on satellite imagery.

Nowadays, decision makers benefit from light detection and ranging (LiDAR) technology, which provides 3-D explicit information for performing the individual tree crown (ITC) segmentation with a high accuracy level. Conventional methods for ITC segmentation degrade the 3-D information of the point cloud into a 2-D image for applying image processing methods, which are based on local maximum filtering [4]. A recent segmentation comparative assessment in [5] remarked the superior performance of the 3-D segmentation algorithms over the methods based on 2-D image. In particular, adaptive 3-D mean shift (AMS3D) [6] clearly outperforms other segmentation approaches.

The mean shift (MS) algorithm [7] is a nonparametric method for finding the maximum value (mode) of a probability density function (PDF). Each LiDAR point contributes to the PDF based on the distribution estimated by the kernel profile. The kernel output is a weighted mean point that is shifted iteratively to locate the mode. A potential ITC is defined by a cluster of points that converge to the same mode. In [8], the kernel profile shape influences consistently in the MS performance. A superellipsoid (SE) kernel profile improved the segmentation and confirmed the findings of Yilmaz [9], who reveals that anisotropic symmetric kernels preserve most of the non-object region outside of the kernel.

Ferraz *et al.* [6] proposed the adaptivity of the kernel profile size in the MS algorithm, known as AMS3D. The allometry equations for estimating the bandwidths of the cylinder kernel are suitable for tropical forests, but this adaptation requires a performance assessment for other forest types. This letter presents a methodology for adapting a SE kernel profile into an ellipsoid crown shape model for temperate forests. Results demonstrate that the ellipsoid adaptation provides better segmentation results for coniferous species with respect to other AMS3D approaches. This work is divided as follows: Section II describes the background of MS algorithm for ITC segmentation, Section III presents the main contribution of this work by adapting a crown shape model, Section IV describes the data sets, the parameters settings and the most important

Manuscript received February 9, 2020; revised June 3, 2020 and June 26, 2020; accepted July 13, 2020. This work was supported by LabEx OSUG@2020 through the Investissements D'avenir under Grant ANR10 LABX56. *(Corresponding author: Eduardo Tusa.)*

Eduardo Tusa is with the Université Grenoble Alpes, INRAE, LESSEM, 38000 Grenoble, France, also with CNRS, Grenoble INP, Institute of Engineering, Université Grenoble Alpes, GIPSA-Lab, 38000 Grenoble, France, and also with the Universidad Técnica de Machala, Facultad de Ingeniería Civil, AutoMathTIC, Machala 070210, Ecuador (e-mail: etusa@utmachala.edu.ec).

Jean-Matthieu Monnet and Jean-Baptiste Barré are with the Université Grenoble Alpes, INRAE, LESSEM, 38000 Grenoble, France.

Mauro Dalla Mura is with CNRS, Grenoble INP, Institute of Engineering, Université Grenoble Alpes, GIPSA-Lab, 38000 Grenoble, France, and also with the Tokyo Tech World Research Hub Initiative (WRHI), School of Computing, Tokyo Institute of Technology, Tokyo 152-8550, Japan.

Michele Dalponte is with the Department of Sustainable Agro-Ecosystems and Bioresources, Research and Innovation Centre, Fondazione Edmund Mach, 38010 San Michele all'Adige, Italy.

Jocelyn Chanussot is with CNRS, Grenoble INP, Institute of Engineering, Université Grenoble Alpes, GIPSA-Lab, 38000 Grenoble, France.

Color versions of one or more of the figures in this letter are available online at http://ieeexplore.ieee.org.

Digital Object Identifier 10.1109/LGRS.2020.3012718

results and finally, Section V corresponds to the conclusions and the work perspectives.

II. MS Segmentation

If we consider a 3-D point coordinate $\mathbf{x_i} = (X_i, Y_i, Z_i)$, the MS vector, $\mathbf{v}(\mathbf{x_i})$, is given by the following equation:

$$\mathbf{v}(\mathbf{x_i}) = \frac{\sum_{\mathbf{x_j} \in N(\mathbf{x_i})} K(\mathbf{x_i}, \mathbf{x_j})\mathbf{x_j}}{\sum_{\mathbf{x_j} \in N(\mathbf{x_i})} K(\mathbf{x_i}, \mathbf{x_j})} - \mathbf{x_i} \tag{1}$$

where $N(\mathbf{x_i})$ represents a set of points $\mathbf{x_j}$ in the neighborhood of $\mathbf{x_i}$ described by the kernel profile, and $K(\mathbf{x_i}, \mathbf{x_j})$ is the kernel function that weights the importance of each point $\mathbf{x_j}$ through a parameter called bandwidth. The selection of the kernel profile shape, weight, and size has important variations that are studied in Sections II-A–II-C.

A. Kernel Profile Shape

The kernel profile shape defines the distribution of the points $\mathbf{x_j}$ in the neighborhood of $\mathbf{x_i}$. Ferraz *et al.* [10] use a straightforward implementation based on a cylinder of radius r_{kc} and height h_k. Xiao *et al.* [8] proposed the SE profile, $N(\mathbf{x_i})$, in (2) for selecting the set of points $\{\mathbf{x_j} \in N(\mathbf{x_i}) | N(\mathbf{x_i}) \leq 1\}$

$$N(\mathbf{x_i}) = \frac{\left\|\mathbf{x_i^h} - \mathbf{x_j^h}\right\|^n}{r_k^n} + \frac{\|Z_i - Z_j\|^n}{a_k^n} \tag{2}$$

where $\mathbf{x_i} = (\mathbf{x_i^h}, Z_i)$ and $\mathbf{x_i^h} = (X_i, Y_i)$ represent the 2-D components of $\mathbf{x_i}$, and $\mathbf{x_j} = (\mathbf{x_j^h}, Z_j)$ is a point in the neighborhood formed by the SE kernel profile with center at $\mathbf{x_i}$, a_k is the radius of the intersection of the kernel profile with the z-axis, r_k is the radius of the kernel profile circle in the xy-plane, and n is a positive real number that determines the shape of the kernel profile. An ellipsoid emerges when $n = 2$, and it becomes a cone when n decreases to 1.

B. Kernel Profile Weight

Following the multivariate kernel proposed by Comaniciu and Meer [7] for image segmentation, the kernel weight $K(\mathbf{x_i}, \mathbf{x_j})$ proposed by Ferraz *et al.* [10] is given in the following equation:

$$K(\mathbf{x_i}, \mathbf{x_j}) = K_h\left(\mathbf{x_i^h}, \mathbf{x_j^h}, w_h\right) K_z(Z_i, Z_j, w_z) \tag{3}$$

where K_h is the horizontal kernel weight, K_z is the vertical kernel weight, w_h and w_z are their respective bandwidths, which depend on the kernel profile shape. Ferraz *et al.* [10] use the Gaussian function for the horizontal kernel weight and Epanechnikov function, K_z^F, for the vertical kernel weight. Another combination is proposed by Xiao *et al.* [8] whose horizontal kernel weight, K_h, is a Gaussian function with normal distribution and the vertical kernel, K_z^X, is weighted on higher points to converge at the top of a tree.

C. Kernel Profile Size

Following the tree size allometry equations, Ferraz *et al.* [6] computed the radius r_{kc} and the height h_k of the cylinder kernel profile, by using the following equations:

$$r_{\mathrm{kc}} = m_1 Z_i \tag{4}$$

$$h_k = m_2 Z_i \tag{5}$$

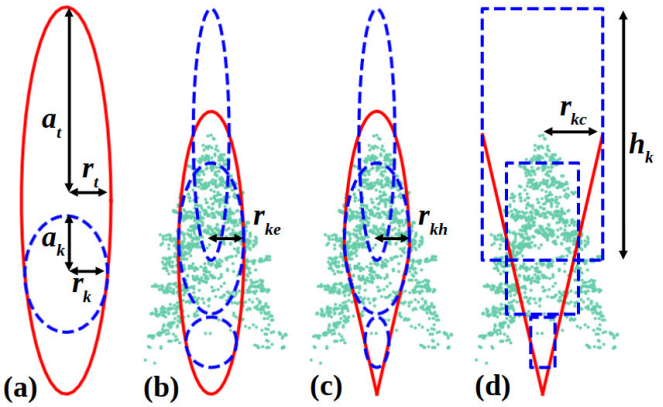

Fig. 1. Three different crown shape models in red line: (a) and (b) ellipsoid, (c) hybrid model, and (d) inverted cone. Two kernel profiles in dotted blue line: SE in (a)–(c), and cylinder in (d). In (a), we illustrate the parameters of the ellipsoid crown model and the SE kernel profile.

where m_1 represents the slope of the linear regression between the tree height and the crown radius, and m_2 is the slope between the tree height and the crown depth. In Fig. 1(d), this kind of adaptive kernel size leads to fit an inverted cone as long as it moves on the z-axis. Although this approach has been assessed for tropical forests by dealing with wide crowns, coniferous trees that are present in temperate forests, are better described by narrow clusters in the upper parts of the canopy. As a consequence, the inverted cone approach would lead to an undersegmentation effect by merging adjacent coniferous tree crowns. An alternative solution to this problem is presented by Xiao *et al.* [8] by testing different profile sizes with and without adapting the kernel profile size. In this work, we compare the previous strategies for controlling the kernel profile size with our AMS3D approach.

III. AMS3D Based on Crown Shape Model

Our objective is to adapt the SE kernel profile size by fitting it into an ellipsoid crown model, using the parameters m_1 and m_2 [Fig. 1(a)]. If the tree crown model is defined by the crown radius r_t in the xy-plane and the radius of the intersection of the crown model along the z-axis, a_t, it is possible to derive the parameters of the SE kernel profile r_k and a_k as it is illustrated in Fig. 1(a). Previously, a preprocessing stage is applied in the 3-D point cloud by removing the points less than $h_{\min} = 1.5$ m [11]. The negative effects of shrubs, grassland, and low height objects are avoided by applying this threshold.

The main core of AMS3D is described in Algorithm 1. The algorithm is initialized with a point $\mathbf{x_i}$ and a set of parameters $m = \{m_1, m_2\}$. The output variable $\mathbf{u_i}$ is the mode derived from $\mathbf{x_i}$. The kernel parameters r_k and a_k are initialized by (4) and (5), respectively. The parameter a_k is assumed to be half of the cylinder height h_k. These parameters determine the neighborhood $N(\mathbf{u_i})$ by using (2) and to estimate the weighted mean $\mathbf{u_{i+1}}$. If the euclidean distance, Δ_u, between $\mathbf{u_{i+1}}$ and $\mathbf{u_i}$ is less than 1×10^{-7} (threshold selected empirically), then MS vector [see (1)] converges and $\mathbf{u_{i+1}}$ becomes a mode. This is recorded and the next point $\mathbf{x_{i+1}}$ is evaluated. If not, a new MS vector is recomputed, $\mathbf{u_i} = \mathbf{u_{i+1}}$, until it converges.

The incorporation of the crown shape model for controlling the kernel size is executed when the MS vector does not

Algorithm 1: AMS3D With Ellipsoid Crown Model

Input: $\mathbf{x_i}$ - 3D LiDAR point.
Parameter: m_1 and m_2 - Allometry coefficients.
Data: $\{\mathbf{x_i}, \ldots, \mathbf{x_N}\}$ - 3D point cloud.
Output: $\mathbf{u_i}$ - Mode of the point $\mathbf{x_i}$.
for *i = 1,..,N* **do**
  Initialize $\mathbf{u_i} \leftarrow \mathbf{x_i}$, $r_k \leftarrow m_1 Z_i$, $a_k \leftarrow \frac{1}{2} m_2 Z_i$, and $\Delta_u \leftarrow 10^7$;
  while $\Delta_u \geq 10^{-7}$ **do**
    $\mathbf{u_{i+1}} \leftarrow \frac{\sum_{\mathbf{u_j} \in N(\mathbf{u_i})} K(\mathbf{u_i}, \mathbf{u_j}) \mathbf{u_j}}{\sum_{\mathbf{u_j} \in N(\mathbf{u_i})} K(\mathbf{u_j}, \mathbf{u_i})}$;
    $\Delta_u \leftarrow ||\mathbf{u_{i+1}} - \mathbf{u_i}||$;
    $\mathbf{u_i} \leftarrow \mathbf{u_{i+1}}$;
    if $\Delta_u \geq 10^{-7}$ **then**
      $h_{max} \leftarrow \max_{\mathbf{u_j} \in C(\mathbf{u_i})}(Z_j)$;
      Compute a_t and r_t according to (6) and (7);
      Compute r_{ke} according to (9) ;
      Update $r_k \leftarrow r_{ke}$ and $a_k \leftarrow \frac{1}{2} m_2 Z_i$;
    else
      break;

converge ($\Delta_u \geq 1 \times 10^{-7}$). The point of maximum height $h_{\max}$ is searched in the cylindrical neighborhood $C(\mathbf{u_i})$ of radius r_k and infinite height. The tree crown parameters r_t and a_t are obtained from the following equations:

$$a_t = \frac{1}{2}(h_{\max} + h_{\min}) \tag{6}$$

$$r_t = (h_{\max})^{\alpha}. \tag{7}$$

Equation (7) comes from the allometry relationship between the tree height and the crown radius used for 3-D ITC segmentation [12]. The parameter α is estimated by equating the expressions (4) and (7), when $Z_i = a_t$. This means that the kernel profile radius should be equal to the tree crown radius around half of the tree height. It turns out the following equation:

$$\alpha = \frac{\log(m_1 a_t)}{\log(h_{\max})}. \tag{8}$$

Once the parameters a_t and r_t are obtained, the kernel radius, r_{ke}, from the ellipsoid crown model [Fig. 1(b)] that controls the radius r_k [Fig. 1(a)] from the SE kernel from (2), is derived from the following ellipse equation:

$$r_{\text{ke}} = \frac{r_t}{a_t} \sqrt{2 a_t Z_i - Z_i^2}. \tag{9}$$

The parameter a_k is updated based on the new estimation of Z_i, and $r_k = r_{\text{ke}}$. In addition to the ellipsoid crown model, a hybrid crown model [Fig. 1(c)] is implemented by using the same a_k parameter and by computing a hybrid kernel radius value $r_{kh} = \min(r_{kc}, r_{\text{ke}})$ in order to set $r_k = r_{kh}$.

IV. Experimental Analysis

For the experimental setup, Table I presents a description of six different AMS3D models assessed in this work. Model F represents the adaptive approach of Ferraz *et al.* [6] with cylinder (C) kernel profile [Fig. 1(d)]. The remaining models implement the (SE) kernel profile from (2). Model X represents the approach of Xiao *et al.* [8] which has two parameters, r_k and b, for estimating $a_k = b \times r_k$, but no kernel size adaptation. Models E1 and E2 introduce the ellipsoid crown model [Fig. 1(b)], while models H1 and H2 implement the hybrid crown model [Fig. 1(c)], with $n = \{1.5, 2.0\}$.

TABLE I
AMS3D Configurations Based on the Kernel Profile

AMS3D Model	Shape		Weight		Size	
	Type	n	K_h	Vertical	Radius	Height
F [6]	C	-	$\gamma = 5.0$	K_z^F	r_{kc}	h_k
X [8]	SE	1.5	$\gamma = 0.5$	K_z^X	r_k	a_k
E1	SE	1.5	$\gamma = 5.0$	K_z^F	r_{ke}	a_k
E2	SE	2.0	$\gamma = 5.0$	K_z^F	r_{ke}	a_k
H1	SE	1.5	$\gamma = 5.0$	K_z^F	r_{kh}	a_k
H2	SE	2.0	$\gamma = 5.0$	K_z^F	r_{kh}	a_k

TABLE II
Summary of the Field Measurements at Tree Level

Study site (No. Plots)	No. Tree Crown	Average DBH $[cm]$	Average Tree Height $[m]$	Average Crown Area $[m^2]$	Species CON [%]	Species BRO [%]
Chamrousse (7)	894	26.2	14.8	23.3	79.8	20.2
Pellizzano (15)	543	29.4	19.6	17.8	87.8	12.2

For the algorithm evaluation, the cluster points detected as a potential tree from each algorithm are projected into the xy-plane for computing the 2-D centroid and for fitting an ellipsoidal crown shape. For every detected tree, we pair with a tree in the inventory based on the matching index, I_{TC}, which is the ratio of the distance between the assumed tree top and detected maxima, and the matching distance described in [4]. This index is multiplied by the Jaccard distance $J_d = 1 - J_i$, where J_i is the Jaccard index equal to $((V_R \cap V_D)/(V_R \cup V_D))$, V_R and V_D are the tree volume from reference (ground truth inventory) and from detections, based on the ellipse area and the tree height. When the potential pair with the lowest matching factor $J_d \times I_{\text{TC}}$ is validated, the lists of remaining detected and reference trees are updated before moving to the next pair. The number of matched trees are called true positives (TP), N_R is the number of reference trees in the inventory and N_D is the number of detected trees. Then, three metrics are computed: Recall $= \text{TP}/N_R$, Precision $= \text{TP}/N_D$, and F1-score.

A. Data Set

The characteristics of 1437 trees from two study sites [13] are summarized in Table II with average values of: diameter at breast height (DBH), tree height, and crown area. The percentage of conifers (CON) and broadleaves (BRO) are also reported. Chamrousse site is located in Belledonne massif, Northern Alps, France. Seven plots were used: four of size of 50×50 m^2, two circular plots of 15 m radius, and a plot of 80×100 m^2, which is part of a long-term inventory data set [14]. The forest is dominated by Norway spruce (*Picea abies*; 37.5%) and other conifers: silver fir (*Abies alba*; 31.6%) and mountain pine (*Pinus uncinata*; 10.6%); broadleaves species are mainly represented by European beech (*Fagus sylvatica*; 15.2%). Tree crown extensions are measured with

ruban tapes in the north, south, east and west directions as the horizontal distance between the trunk center and the vertical projection of the furthest live branch along that direction. The airborne laser scanning (ALS) data was collected between June 21st and 23rd, 2018, by using a RIEGL LMS-Q780 sensor, obtaining a mean pulse density of 20 pulses m^{-2}.

The second site is located in the municipality of Pellizzano in the Italian Alps [11]. In this site, 15 circular plots were measured: six plots have radius of 15 m and the remaining ones have 20 m radius. Tree crown was derived from the field-measured distances in the four cardinal directions from the trunk center to the crown boundary assuming an ellipsoidal shape. The complex forest structure is formed by coniferous trees: 75.7% of Norway spruce, 9.8% of larch (*Larix decidua*) and small proportions (more than 10 trees) of broadleaves such as silver birch (*Betula pendula*) and common alder (*Alnus glutinosa*). ALS data were carried out between September 7th and 9th, 2012, by using a RIEGL LMS-Q680i sensor with a mean pulse density of 60 pulses m^{-2}.

B. Parameters

For the algorithms F, E1, E2, H1, and H2; the parameters m_1 and m_2 are computed for every plot on the basis of the ground truth information. For every linear regression, we obtain two confidence intervals (CI) at 95.0% and 99.9% for generating a set of 5 values per parameter: the slope value, the upper and lower limits of the two CI. In this way, we run 25 experiments per algorithm in each plot. The mean value of parameter m_1 is 0.131 with minimum and maximum values between 0.025 and 0.316. The parameter m_2 has a mean value of 0.786 with minimum and maximum values between 0.143 and 0.969. The parameters for the model X are selected according to [8], where $r_k = \{2, 3\}$ and $b = \{1, 1.5, 2, 2.5, 3\}$.

C. Results and Discussion

The overall performance of six AMS3D segmentation schemes are summarized in Table III based on four metrics: average J_i, recall, precision, and F1-score. The best results per plot were selected according to the parameter setting with the maximum F1-score. Although F1-score values were similar among the algorithms with ellipsoid and hybrid crown model, the algorithm E1 presented the highest recall, i.e., the greatest amount of matched trees, and the highest average J_i, i.e., the best ITC segmentation. Algorithm F produced undersegmented tree crowns because the kernel radius enclosed more than one tree at upper layers. This issue is solved in our method by adjusting the crown radius. Algorithm X maximized F1-score by decreasing the number of detections, which produced the best precision with respect to other algorithms, but it decreased the number of TP trees. This algorithm produced better recall values with small kernels by oversegmenting the point cloud.

The algorithm E1 is assessed in each study site to remark differences of the point density. The recall values in the sites of Chamrousse and Pellizzano were 56.6% and 63.0%, respectively. Although the pulse density of Pellizzano site is three times Chamrousse's pulse density, the recall difference between these two sites did not respond in that magnitude. Other factors described in Table II can contribute for

TABLE III

OVERALL ASSESSMENT OF SIX AMS3D SCHEMES BASED ON 22 FOREST PLOTS FROM TWO STUDY SITES

AMS3D	J_i [%]	Recall [%]	Precision [%]	F1-score [%]
F [6]	49.1	46.1	72.0	56.2
X [8]	48.5	52.8	74.3	61.7
E1	**53.7**	**59.0**	67.4	62.9
E2	52.2	57.1	70.7	63.1
H1	52.6	58.2	67.3	62.4
H2	52.3	58.0	68.4	62.8

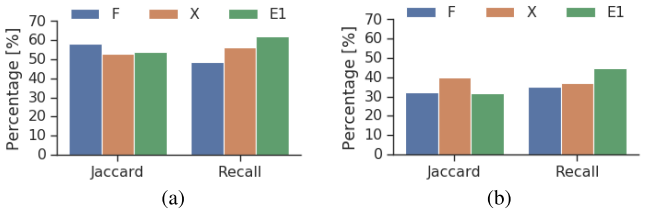

Fig. 2. Algorithm comparison assessment based on species: (a) 1190 conifers and (b) 247 broadleaves from the sites in Pellizzano and Chamrousse.

E1 to deliver better performance in Pellizzano. For instance, the average tree height is greater in Pellizzano than Chamrousse, presenting more salient trees which are easy to be segmented. Also, the Pellizzano site has 8.0 points of percentage more conifers than Chamrousse site.

For the species analysis, an important finding of the algorithm performances is presented in Fig. 2, which corresponds to the results of the segmentation for coniferous and broadleaves species. In Fig. 2(a), E1 obtains the highest recall of 62.0% for conifers by reaching a difference of 5.9 points of percentage over the algorithm X and 13.6 over F. This difference is compensated for algorithm F that had the best J_i: 58.2%, 3.8 points of percentage better than algorithm E1. For broadleaves [Fig. 2(b)], none of the presented algorithms performed a recall over 50.0% and J_i better than 40.0%.

For discussing the species results at plot level, two conifers plots and two forest plots with more than 50% of broadleaves are selected from both study sites. The histogram of heights are computed by setting a bin size of 5 m for TP, false negative (FN) and false positive (FP) tree detections. In addition, the estimation of the gap area can be used as a forest structure descriptor. The gap area percentage (GAP) is estimated from the rate between the gap area given by a height threshold every 1 m and the maximum gap area surface (approximately the forest plot surface) calculated in an R package *ForestGapR* [15]. The resulting curve overlaps each height histogram in Fig. 3.

In Fig. 3, plot 5 from Pellizzano, PP5, [Fig. 3(a)] and plot 3 from Chamrousse, PC3, [Fig. 3(b)] obtained the highest recalls: 100% and 72.7%, respectively. PP5 revealed the ideal scenario for ITC segmentation. E1 detected all the 21 conifers (small plot), whose heights were greater than 20 m (salient trees). As the GAP curve increased, the number of TP and FP trees increased, because tree crowns became more sparse when the GAP value overpasses 20.8%. The forest structure of conifers has more sparse upper canopy layers with prominent gap areas. In contrast to PP5, the majority of trees in PC3 are less than 20 m (Fig. 4).

Although PC3 showed a GAP value of 36.5% at 5 m, E1 faced difficulties to segment understory trees because the

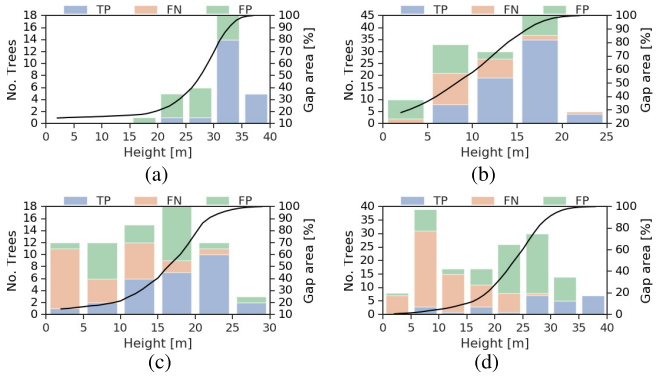

Fig. 3. Histograms of heights for the TP, FN, and FP trees in the conifers plots: (a) plot 5 from Pellizzano (PP5) and (b) plot 3 from Chamrousse (PC3). Below, the plots with more than 50% of broadleaves: (c) plot 1 from Pellizzano (PP1) and (d) plot 1 from Chamrousse (PC1). The GAP curve is represented in black.

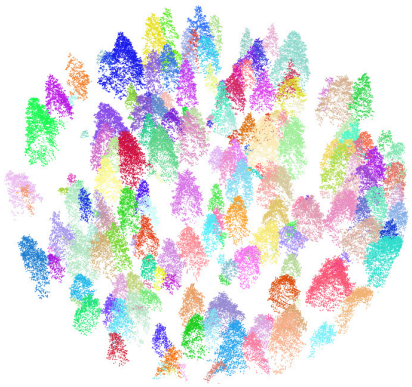

Fig. 4. 3-D segmentation of PC3 by using algorithm E1. 66 trees out of 92 were matched, resulting in a recall of 71.7% and a Jaccard index of 54.5%.

crown shape model that controls the kernel size is calibrated with the height of the highest point, which makes it suitable for salient trees. In Fig. 3, plot 1 from Chamrousse, PC1, [Fig. 3(d)] and plot 1 from Pellizzano, PP1, [Fig. 3(c)] obtained lower recalls: 29.3% and 54.9%, respectively. Two aspects are remarked in these plots. First, most of the trees are located at the lower canopy layers (tree heights less than 20 m). It increased the amount of FN trees with respect to the conifers plots. Second, the canopy of these plots is dense with low GAP values at the lower canopy layers: 1.5% at 5 m in PC1 and 14.6% at 2 m in PP1. This makes it difficult to segment groups of understory trees that belong to the same species because a dense point cloud can lead to undersegmentation. If the LiDAR point density is very low, the clusters that represent potential ITC become noisy and have low definition to be delineated.

V. Conclusion

In this letter, we presented an AMS3D approach for ITC segmentation by adapting the kernel profile size through crown shape model and by exploring the optimal parameters. The ellipsoid crown shape model with a SE kernel profile of $n = 1.5$ presents the best overall recall of 59.0% and Jaccard index of 53.7% among the assessed schemes of 3-D segmentation. The most outstanding results of the algorithm are revealed for the coniferous trees. Forest plots with a high presence of broadleaves trees represent challenging tasks for all ITC segmentation approaches. Future work is going to be focused on estimating automatically the algorithm parameters in order to consolidate a tool for end-user purposes. This task will involve the integration with other data modalities, such as hyperspectral imaging for tree species prediction.

References

[1] E. Bergseng, H. O. Ørka, E. Næsset, and T. Gobakken, "Assessing forest inventory information obtained from different inventory approaches and remote sensing data sources," *Ann. Forest Sci.*, vol. 72, no. 1, pp. 33–45, Jan. 2015.

[2] H. Hamraz, M. A. Contreras, and J. Zhang, "A robust approach for tree segmentation in deciduous forests using small-footprint airborne LiDAR data," *Int. J. Appl. Earth Observ. Geoinf.*, vol. 52, pp. 532–541, Oct. 2016.

[3] T. W. Crowther *et al.*, "Mapping tree density at a global scale," *Nature*, vol. 525, no. 7568, pp. 201–205, 2015.

[4] J.-M. Monnet, E. Mermin, J. Chanussot, and F. Berger, "Tree top detection using local maxima filtering: A parameter sensitivity analysis," in *Proc. 10th Int. Conf. LiDAR Appl. Assessing Forest Ecosyst. (Silvilaser)*, Freiburg, Germany, Sep. 2010, p. 9.

[5] M. Aubry-Kientz *et al.*, "A comparative assessment of the performance of individual tree crowns delineation algorithms from ALS data in tropical forests," *Remote Sens.*, vol. 11, no. 9, pp. 1–21, 2019.

[6] A. Ferraz, S. Saatchi, C. Mallet, and V. Meyer, "LiDAR detection of individual tree size in tropical forests," *Remote Sens. Environ.*, vol. 183, pp. 318–333, Sep. 2016.

[7] D. Comaniciu and P. Meer, "Mean shift: A robust approach toward feature space analysis," *IEEE Trans. Pattern Anal. Mach. Intell.*, vol. 24, no. 5, pp. 603–619, May 2002.

[8] W. Xiao, A. Zaforemska, M. Smigaj, Y. Wang, and R. Gaulton, "Mean shift segmentation assessment for individual forest tree delineation from airborne LiDAR data," *Remote Sens.*, vol. 11, no. 11, pp. 1–19, 2019.

[9] A. Yilmaz, "Object tracking by asymmetric kernel mean shift with automatic scale and orientation selection," in *Proc. IEEE Conf. Comput. Vis. Pattern Recognit.*, Minneapolis, MN, USA, Jun. 2007, pp. 1–6.

[10] A. Ferraz *et al.*, "3-D mapping of a multi-layered Mediterranean forest using ALS data," *Remote Sens. Environ.*, vol. 121, pp. 210–223, Jun. 2012.

[11] K. Kandare, H. O. Ørka, J. C.-W. Chan, and M. Dalponte, "Effects of forest structure and airborne laser scanning point cloud density on 3D delineation of individual tree crowns," *Eur. J. Remote Sens.*, vol. 49, no. 1, pp. 337–359, Jan. 2016.

[12] J. Williams *et al.*, "3D segmentation of trees through a flexible multiclass graph cut algorithm," *IEEE Trans. Geosci. Remote Sens.*, vol. 58, no. 2, pp. 754–776, Feb. 2020.

[13] E. Tusa *et al.*, "Fusion of hyperspectral imaging and LiDAR for forest monitoring," in *Hyperspectral Imaging* (Data Handling in Science and Technology), vol. 32, J. M. Amigo, Ed. Amsterdam, The Netherlands: Elsevier, 2020, ch. 2.11, pp. 281–303.

[14] M. Fuhr *et al.*, "Long-term tree inventory data from mountain forest plots in France," *Ecology*, vol. 98, no. 4, p. 1180, 2017.

[15] C. A. Silva *et al.*, "Forest gap R: An R package for forest gap analysis from canopy height models," *Methods Ecol. Evol.*, vol. 10, no. 8, pp. 1347–1356, Aug. 2019.